TYC 9291-1051-1: The First Precision Photometry and Analyses of the Active, Totally Eclipsing, Solar-type Binary

Ronald G. Samec
Faculty Research Associate, Pisgah Astronomical Research Institute, 1 PARI Drive, Rosman, NC 28772; ronaldsamec@gmail.comInstitute

Heather Chamberlain
Pisgah Astronomical Research Institute, 1 PARI Drive, Rosman, NC 28772; 4hcham@gmail.com

Walter Van Hamme
Department of Physics, Florida International University, Miami, FL 33199; vanhamme@fiu.edu

Received March 31, 2020; revised May 15, 2020; accepted July 22, 2020

Abstract CCD Bessell BVRI light curves of TYC 9291-1051-1 were taken on 9, 20, and 28 August 2019 in remote mode at Cerro Tololo InterAmerican Observatory with the 0.6-m SARA South reflector by R. Samec and W. Van Hamme. The variability of TYC 9291-1051-1 (UNSW V-633) was discovered by the University of New South Wales Extrasolar Planet Search (Christiansen *et al.* 2008), which classified it as an EW variable with a magnitude of V = 10.90 and a period of 0.42713 d. Five times of minimum light were determined from our present observations, which include two primary eclipses and three secondary eclipses. Linear and quadratic ephemerides were determined from all available times of minimum light. A ~13.3-year period study (~11,400 orbits) reveals that the period is increasing. This could be due to mass transfer making the mass ratio more extreme. Wilson-Devinney analyses reveals that the system is a A-type W UMa binary (P-shift = 0.5) with a mass ratio that is somewhat extreme, $M_2/M_1 = 0.260 \pm 0.004$ (star 1 is the more massive component, $M_1/M_2 = 3.8$). The total eclipse makes this a good determination (Terrell and Wilson 2005). Its Roche lobe fill-out is ~32%. The solution has two major spot regions, a mid-latitude cool spot of radius 19 ± 5 degrees and an equatorial weak hot spot (T-factor = 1.06) of 21 ± 6 degrees. We note that the hot spot is on the on the gainer which covers the Lagrangian, L1, point. This probably has to do with the mass transfer. The spot regions were variable during the 19-day interval of observation. The temperature difference of the components is about ~270 K, with the more massive component as the hotter one, so it is an A-type W UMa binary. The inclination is 83.25 ± 0.50°. The primary (with P-shift 0.5) minimum has a time of constant light with an eclipse duration of 13.3 minutes.

1. Active solar-type contact binaries

W UMa binaries are believed to be undergoing steady but slow angular momentum losses due to magnetic braking as stellar winds blow radially away on stiff bipolar field lines. The secondary component is decreasing in mass as it is absorbed by the primary component. They are usually highly evolved A-type W UMa binary stars (primary component is hotter) and are believed to be among the most ancient stars. These binaries eventually coalesce into blue straggler type, single, fast rotating A-spectral type stars (Guinan and Bradstreet 1988). Most are spotted and magnetically active as would be expected for short period solar-type binaries. See Figure 1. Twenty-five highly evolved extreme mass ratio binaries in this rare group are summarized in Samec *et al.* (2011). We explore another solar-type binary, TYC 9291-1051 in this paper.

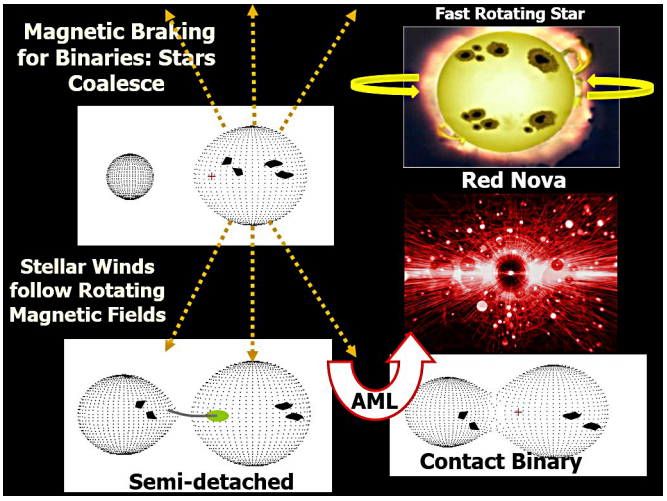

Figure 1. Depiction of a binary star made up of two solar-type stars undergoing magnetic braking which results in angular momentum loss (AML). Plasmas leave along North and South magnetic field lines, causing the magnetically active binary (detached spotted binary in the upper left-hand corner) to lose angular momentum and steadily fill its Roche lobe and move to a semidetached and then a contact binary configuration. The binary becomes unstable and a Red Novae event (Tylenda and Kamiński 2016) erupts finally resulting in a fast-rotating single star.

2. History, photometric targets, and observations

The variability of TYC 9291-1051-1 (UNSW V-633) was discovered by the University of New South Wales (UNSW) Extrasolar Planet Search (Christiansen *et al.* 2008), which classified it as an EW variable with a magnitude of V = 10.90 and an ephemeris of

$$HJD = 2453866.2150\,d + 0.42713\,d \times E \qquad (1)$$

A plot of UNS V-633 is given in Figure 2.

SIMBAD gives J = 10.44 ± 0.23, K = 10.015 ± 0.22 so J–K = 0.425 ± 0.045. GAIA DR2 gives parallax = 2.779 ± 0.036, Distance = 360 ± 5 pc. Observations of the system are continuously being undertaken by the All-Sky Automated Survey for Super Nova Search Program of Ohio State (ASAS-SN; Shappee *et al.* 2014; Kochanek *et al.* 2017). See Figure 2. The information included V = 12.07, amplitude = 0.54 mag, var. type EW, and an ephemeris:

$$\text{HJD} = 2456817.68537\,\text{d} + 0.4271315\,\text{d} \times \text{E} \qquad (2)$$

The ASAS-SN light curves are given in Figure 3. The preliminary results of this study were reported at the 235th meeting of the American Astronomical Society (Chamberlain *et al.* 2020).

Characteristics of the variable, comparison, and check star are listed in Table 1. The finding chart of the photometric targets is given in Figure 4. These are in the constellation Pavo. B, V light curves and B–V color curves from 9 and 20 August 2019 are shown in Figures 5 and 6.

Our 2019 BVRI light curves were taken on 9, 20, and 28 August 2019 at Cerro Tololo InterAmerican Observatory with the 0.6-m SARA South reflector by R. Samec and W. Van Hamme with a thermoelectrically cooled (–50° C) 2KX2K ANDOR camera with Bessell BVRI filters. Individual observations included 411 in B, 410 in V, 412 in R, and 415 in I. The observations are given in Table 2. The probable error of a single observation was 13 mmag in B and V, 17 mmag in R, and 20 mmag in I. This was evidently due to the strong magnetic activity. The nightly C–K values stayed constant throughout the observing run with a precision of about 1%. Exposure times varied: 75–100s in B, 40–75s in V, and 22–45s in R and I, depending on the time needed to obtain 1% photometry.

3. Period study

Five times of minimum light were determined from our present observations, which include two primary eclipses and three secondary eclipses:

HJD I = 2458705.61464 ± 0.00005, 2458716.71967 ± 0.0005 d

HJD II = 2458705.82757 ± 0.0012, 2458716.50625 ± 0.0037, and 2458724.62166 ± 0.0008 d.

Minima were calculated using a least squares minimization method (Mikulášek *et al.* 2014) to determine the minima for each curve, in B, V, R_c, and I_c. Standard errors were determined from these values. From the ASAS-SN curve, the data were phased with Equation 2. The minima were fit and 5 times of low light were determined. The ephemeris (Equation 2) was also input. A time of minimum light from MNRAS (Christiansen *et al.* 2008) was also used. From all of these, the following linear and quadratic ephemerides were determined:

$$\text{JD Hel Min I} = 2458705.6129 \pm 0.00016\,\text{d} + 0.42712987 \pm 0.00000030 \times \text{E} \qquad (3)$$

$$\text{JD Hel Min I} = 2458705.6151 \pm 0.0009\,\text{d} + 0.4271345 \pm 0.0000006 \times \text{E} + 0.00000000033 \pm 0.00000000004 \times \text{E}^2 \qquad (4)$$

The quadratic and linear residuals are given in Table 3. The plot of the quadratic term overlying the linear residuals of Equation 4 is given in Figure 7.

Using Equation 3, the B, V, R, I magnitudes and B–V, R–I indices were phased and plotted into light curves and color curves for the observing run. They are given in Figures 8 and 9.

The quadratic ephemeris term yields an increasing orbital period of $\dot{P} = 5.47 \times 10^{-7}$ d / yr. If the period change is due to mass transfer to the primary component, the rate is (in a conservative scenario)

$$\frac{dM}{dt} = \frac{\dot{P} M_1 M_2}{3P (M_1 - M_2)} = \frac{-1.45 \times 10^{-7}\, M_\odot}{d}. \qquad (5)$$

4. Light curve characteristics

The B, V, R, I light curves were phased and averaged at each quarter cycle, phases 0.0, 0.25, 0.50, and 0.75, and important differences were tabulated. These are given in Table 4. The night-to-night curves were of good photometric precision, averaging about 1%. The amplitude of the light curve varies from 0.59 to 0.32 mag in B to I. The O'Connell (the difference of maxima) effect, sometimes an indicator of spot activity, averages several times the noise level, 0.027 mag. The differences in minima are small, 0.032–0.058 mag, indicating contact light curves. The B–V color curves fall so very slightly at phase 0.0, and at phase 0.5, which is characteristic of contact binaries. This probably indicates that It is a W UMa contact binary.

5. Temperature

The 2MASS, J–K = 0.425 ± 0.045 for the binary. This corresponds to a G7.5 ± 3.5V eclipsing binary which yields a temperature of 5500 ± 250 K. Binary stars of this type are noted for having convective atmospheres, so spots are expected. In this case, the magnetic activity is especially high.

6. Light curve solution

The B, V, R, and I curves were pre-modeled with BINARY MAKER 3.0 (Bradstreet and Steelman 2002) and fits were determined in all filter bands. The result of the best fit was that of a A-type contact binary with a high fill-out of about 32% with two spots, one cooler and one slightly hotter than the photosphere. The parameters were then averaged and input into a four-color simultaneous light curve calculation using the 2016 Wilson-Devinney (WD) program (Wilson and Devinney 1971; Wilson 1979, 1990, 1994, 2008, 2012; Van Hamme 1998; Van Hamme and Wilson 2007; Wilson *et al.* 2010; Wilson and Van Hamme 2014). The solution was computed in Mode 3 (contact), started with the initial spot parameters and converged to in the solution. Convective parameters g = 0.32, A = 0.5 were used.

Table 1. Information on the stars used in this study.

Star	*Name*	*R.A. (2000)* h m s	*Dec. (2000)*[1] ° ′ ″	*V*	*J–K*
V (Variable)	TYC 9291-1051-1 GSC 9291 1051 2MASS J05194709+7736136 2MASS J18252748-6734471[2] ASAS 182528-6734.8	18 25 26.15064689	–67 34 39.785303135	12.200[3]	0.425 ± 0.045[3]
C (Comparison)	GSC 9291 958 3UC 045-269292	18 26 01.8201	–67 33 19.410	12.66[3]	0.38[3]
K (Check)	GSC 9291 0987	18 25 55.9738	–67 32 25.343	12.47[3]	0.26 ± 0.041[3]

[1] *ICRS (IAU 2013).* [2] *Gaia Collaboration (2006).* [3] *SIMBAD (CDS 2007).*

Table 2. Sample of first ten TYC 9291-1051-1 B, V, R, I observations.

Δ*B*	*HJD 2458700+*	Δ*V*	*HJD 2458700+*	Δ*R*	*HJD 2458700+*	Δ*I*	*HJD 2458700+*
–0.640	5.4525	–0.638	5.4531	–0.727	5.4515	–0.770	5.4485
–0.684	5.4547	–0.760	5.4555	–0.712	5.4536	–0.818	5.4519
–0.626	5.4571	–0.720	5.4579	–0.734	5.4560	–0.795	5.4540
–0.687	5.4594	–0.740	5.4602	–0.790	5.4583	–0.798	5.4564
–0.668	5.4626	–0.779	5.4634	–0.808	5.4614	–0.783	5.4587
–0.673	5.4650	–0.769	5.4659	–0.834	5.4639	–0.842	5.4618
–0.725	5.4675	–0.772	5.4683	–0.825	5.4664	–0.809	5.4643
–0.722	5.4700	–0.779	5.4708	–0.807	5.4689	–0.813	5.4668
–0.738	5.4725	–0.788	5.4733	–0.827	5.4713	–0.849	5.4692
–0.730	5.4749	–0.810	5.4758	–0.865	5.4738	–0.851	5.4717

Note: First ten data points of TYC 9291-1051-1 B, V, R, I observations.
The full table is available through the AAVSO ftp site at ftp://ftp.aavso.org/public/datasets/samec482-tyc9291.txt (if necessary, copy and paste link into the address bar of a web browser).

Table 3. TYC 9291-1051-1 period study quadratic and linear residuals.

	Epoch HJD 2400000+	*Cycle*	*HJD Linear Residual*	*HJD Quadratic Residual*	*WT*	*HJD Error*	*Reference*
1	51870.9100	–16001.5	0.0157	0.0038	0.05	—	Watson *et al.* 2014 (VSX)
2	53866.2150	–11330.0	–0.0165	–0.0082	0.05	—	Christiansen, *et al.* (2008)
3	56817.6854	–4420.0	–0.0135	–0.0017	0.05	—	Shappee *et al.* 2014; Kochanek *et al.* 2017 (ASAS-SN EPOCH)
4	57154.7031	–3631.0	–0.0012	0.0090	0.02	—	Shappee *et al.* 2014; Kochanek *et al.* 2017 (ASAS-SN)
5	57236.4974	–3439.5	–0.0023	0.0075	0.02	—	Shappee *et al.* 2014; Kochanek *et al.* 2017 (ASAS-SN)
6	57573.7158	–2650.0	–0.0029	0.0048	0.02	—	Shappee *et al.* 2014; Kochanek *et al.* 2017 (ASAS-SN)
7	57867.7999	–1961.5	0.0022	0.0078	0.02	—	Shappee *et al.* 2014; Kochanek *et al.* 2017 (ASAS-SN)
8	58024.5577	–1594.5	0.0034	0.0077	0.02	—	Shappee *et al.* 2014; Kochanek *et al.* 2017 (ASAS-SN)
9	58705.6146	0.0	0.0018	–0.0005	1.00	0.0003	Present observations
10	58705.8276	0.5	0.0011	–0.0011	1.00	0.0021	Present observations
11	58716.5063	25.5	0.0016	–0.0008	1.00	0.0003	Present observations
12	58716.7197	26.0	0.0014	–0.0010	1.00	0.0018	Present observations
13	58724.6217	44.5	0.0015	–0.0010	1.00	0.0001	Present observations

The parameters with errors were allowed to iterate during the light curve modeling. The mass ratio was found to be 0.26. The two spots did converge with some changes as expected, with T-factor of 0.87 and a mid-latitude position and an equatorial spot, very near L1) with T-factor = 1.06. The eclipses are total, so there was a time of constant light in the first eclipse (see Figure 8). A P-shift = 0.5 was inserted so that the WD contact mode would run more smoothly. This means that the primary eclipse is actually the secondary eclipse. But since the eclipses are so close in amplitude, this makes little difference in the interpretation. The parameters carrying an error were the ones that were iterated as the program ran; the others remained fixed in the code.

The light curve solution follows as Table 5. The fill-out was 31.5%. The inclination is 83.25 ± 0.50°. The difference of component temperatures was about 220 K, confirming that the components are in good thermal contact. The total eclipse duration is 13.3 minutes. The modeled period was 0.42710 d. The B, V, R, and I solution curves overlaying the data are given as Figure 10. The geometrical surface representations of TYC9291-1051-1 are shown with spots by orbital phases, 0.0, 0.25, 0.5, and 0.75 in Figure 11 a–d.

7. Discussion

TYC 9291-1051-1 is a A-type contact W UMa binary star. The period increase is probably due to the mass ratio becoming more extreme, so there is a continuous mass exchange with the primary component being the gainer. The hot spot in the neck of the binary may indicate such a mass exchange. The spectral type is that of a solar type with a surface temperature of 5500 K for the less massive component. The higher mass component has a temperature of ~5770 K (G2V). The mass ratio is 0.26, with an amplitude of 0.59–0.52 mag in B to I, respectively. The inclination is 83.25°, which results in a total eclipse at phase 0.0. The A-type W UMa is thought to be near the end of the contact binary phase. This is because the fill-out is unusually high. Very few A-types are in shallow contact (~0–10%). High fill-out means the stars are nearer reaching the maximum fill-out where mass can leave the binary system via the L2 point (see Figure 12).

The Roche lobe surface outlines for TYC 9291-1051-1 are displayed in Figure 13. Note the degree of fill-out.

8. Conclusion

Our period study of this contact W UMa binary has a 13.3-year time duration. The period is found to be strongly increasing at about the five-sigma level. This is due to mass is transferring to the more massive component. AML is also in progress. If this scenario continues, the system will reach an instability and a red novae coalescence event will take place. The system will become a rather normal, fast rotating, single ~F8V type field star (Tylenda and Kamiński 2016).

Table 4. Light curve characteristics for TYC 9291-1051-1.

Filter	*Phase 0.0*	*Mag ± σ* Max I*	*Phase 0.25*	*Mag ± σ* Max II*
B		–0.213 ± 0.005		–0.801 ± 0.010
V		–0.296 ± 0.006		–0.857 ± 0.008
R		–0.327 ± 0.008		–0.901 ± 0.010
I		–0.393 ± 0.007		–0.908 ± 0.028
Filter	*Phase 0.5*	*Mag ± σ* Min II*	*Phase 0.75*	*Mag ± σ* Min I*
B		–0.245 ± 0.006		–0.799 ± 0.006
V		–0.329 ± 0.010		–0.830 ± 0.035
R		–0.368 ± 0.006		–0.828 ± 0.014
I		–0.451 ± 0.010		–0.915 ± 0.008

Filter	*Min I – Max I ± σ*	*Max I – Max II ± σ*	*Min I – Min II ± σ*
B	0.588 ± 0.015	–0.002 ± 0.016	0.032 ± 0.011
V	0.562 ± 0.014	–0.027 ± 0.043	0.033 ± 0.016
R	0.574 ± 0.018	–0.073 ± 0.024	0.040 ± 0.014
I	0.515 ± 0.035	0.007 ± 0.036	0.058 ± 0.017

Filter	*Max II – Max I ± σ*	*Filter*	*Min II – Max I ± σ*
B	0.002 ± 0.016	B	0.556 ± 0.016
V	0.027 ± 0.043	V	0.529 ± 0.018
R	0.073 ± 0.024	R	0.534 ± 0.016
I	–0.007 ± 0.036	I	0.457 ± 0.038

**Magnitude is the variable star – comparison star magnitude.*

Table 5. B, V, R_c, I_c Wilson-Devinney program solution parameters for TYC 9291-1051-1.

Parameters	*Values*		
λB, λV, λR, λI (nm)	440, 550, 640, 790		
$g_1 = g_2$	0.32		
$A_1 = A_2$	0.5		
Inclination (°)	83.25 ± 0.50		
T_1, T_2 (K)	5500, 5770 ± 14		
Ω	2.325 ± 0.005		
$q(m_2/m_1)$	0.260±0.004		
Fill-outs: $F_1 = F_2$ (%)	31.5±0.015		
$L1/(L1+L2+L3)_I$	0.737 ± 0.001		
$L1/(L1+L2+L3)_R$	0.732 ± 0.001		
$L1/(L1+L2+L3)_V$	0.725 ± 0.001		
$L1/(L1+L2+L3)_B$	0.709 ± 0.001		
JD_o (days)	2458705.6144 ± 0.0004		
Period (days)	0.42710 ± 0.00005		
P-shift	0.5		
r_1/a, r_2/a (pole)	0.4785 ± 0.0007, 0.2633 ± 0.0015		
r_1/a, r_2/a (side)	0.5199 ± 0.0011, 0.2759 ± 0.0019		
r_1/a, r_2/a (back)	0.5480 ± 0.0014, 0.3201 ± 0.0041		
Spot I, Star 1		*Spot II, Star 1*	
Colatitude (°)	126 ± 10	Colatitude (°)	85 ± 4
Longitude (°)	288 ± 11	Longitude (°)	356 ± 6
Radius (°)	19 ± 5	Radius (°)	21 ± 6
T-factor	0.87 ± 2	T-factor	1.06 ± 0.04

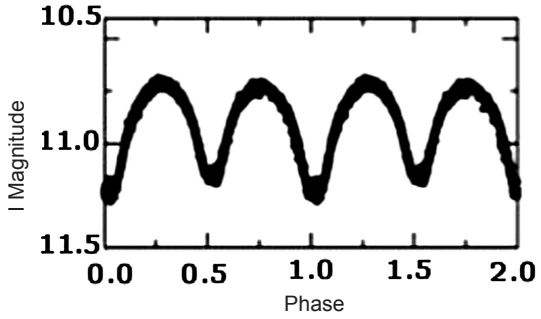

Figure 2. Plot of UNSW V-633, period = 0.42713 d (Christiansen *et al.* 2008). The magnitude is Johnson I.

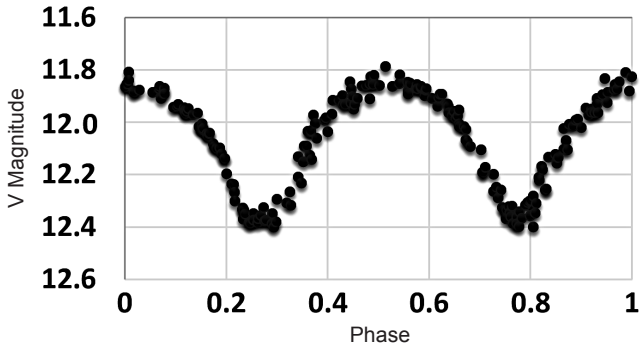

Figure 3. Curves from The ASASSN Site of ASAS J182528-6734.8 (TYC 9291-1051-1; Shappee *et al.* 2014; Kochanek *et al.* 2017).

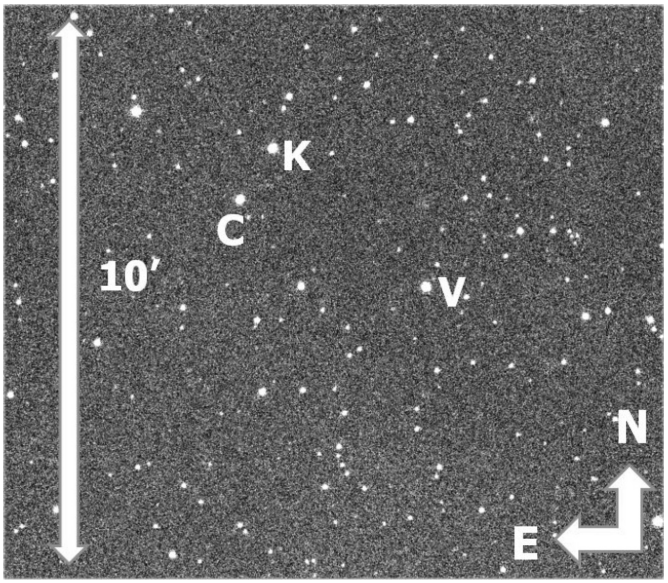

Figure 4. Finding chart of field of TYC 9291-1051-1 using actual image. V, variable, C, comparison star, and K, check star.

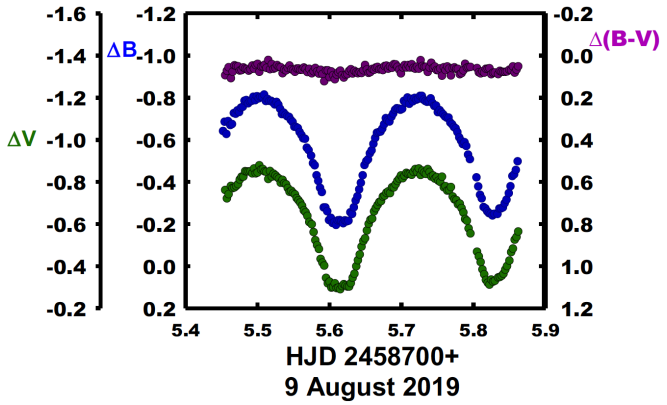

Figure 5. B, V, and B–V color curves of TYC 9291-1051-1 on 9 August 2019.

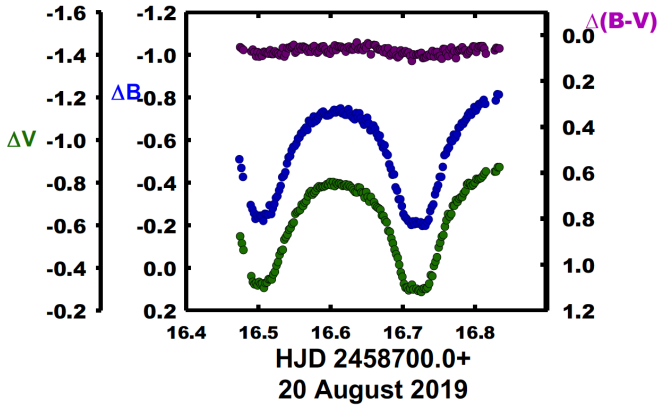

Figure 6. B, V, and B–V color curves of TYC 9291-1051-1 on 20 August 2019.

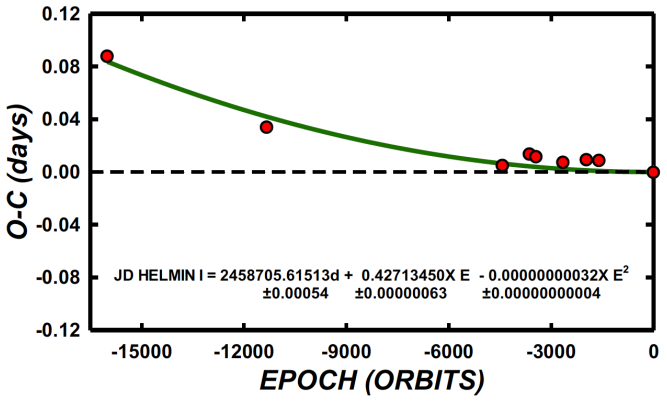

Figure 7. A plot of the quadratic term overlying the linear residuals of Equation 4.

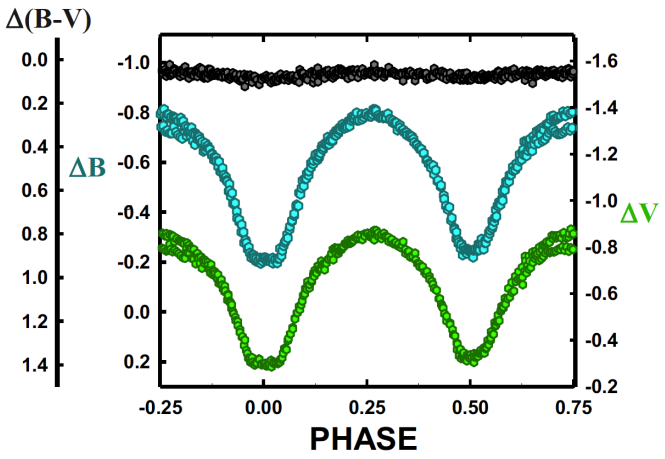

Figure 8. Phased B, V magnitude light curves and color curves (Equation 3). Note the effect of the spots (see phase 0.75) acting over a brief period of 19 days. The change is ~0.08 mag in B and V.

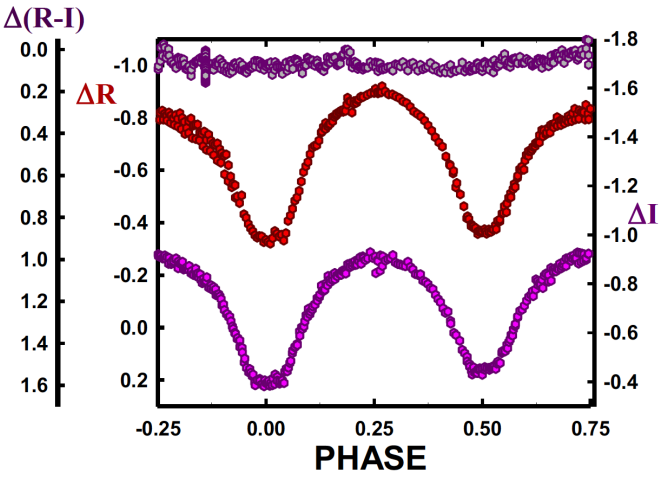

Figure 9. Phased R, I magnitude light curves and color curves (Equation 3). Note the effect of the spots acting over a brief period of 19 days. The shift is ~0.05 mag in R.

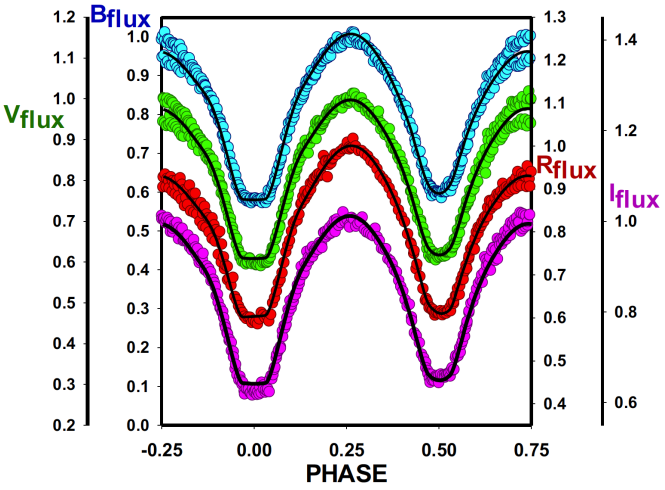

Figure 10. The B, V, R_c, I_c solution curves overlaying the normalized flux data.

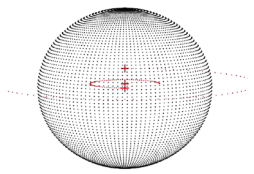

Figure 11a. Geometrical surface representation of TYC9291-1051-1 at phase 0.00.

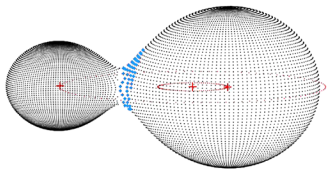

Figure 11b. Geometrical surface representation of TYC9291-1051-1 at phase 0.25. The blue spot is a hot spot.

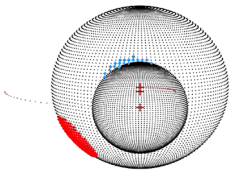

Figure 11c. Geometrical surface representation of TYC9291-1051-1 at phase 0.50. The red spot (on left) is a cool sunspot, the blue spot is a hot spot.

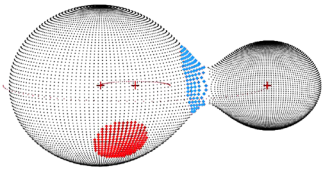

Figure 11d. Geometrical surface representation of TYC9291-1051-1 at phase 0.75. The red spot (on left) is a cool sunspot, the blue spot is a hot spot.

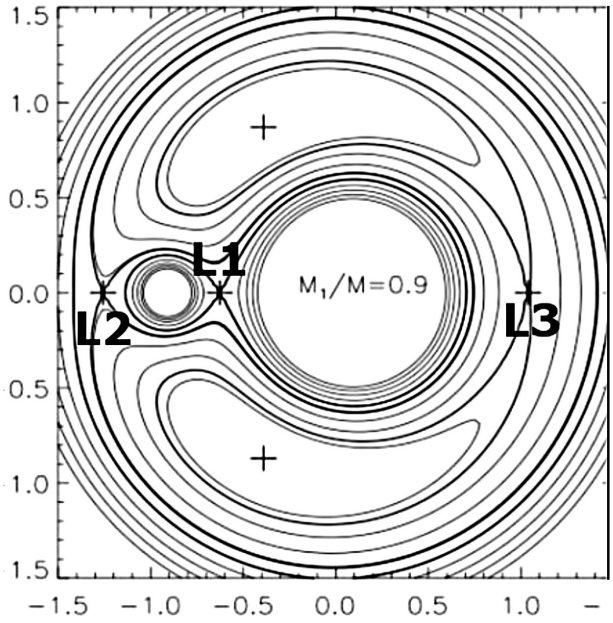

Figure 12. Roche lobe surfaces. Contact binaries have surfaces lying between L1 (fill-out = 0%) and L2 (fill-out = 100%), from http://vitaly.neustroev.net/teaching/2017b/astrophysics_of_interacting_binary_stars_02.pdf (Neustroev 2017). L points added by authors. The unit of the plot of Roche lobe surfaces are $a = a_1 + a_2 = 1$, the normalized semi-major axis.

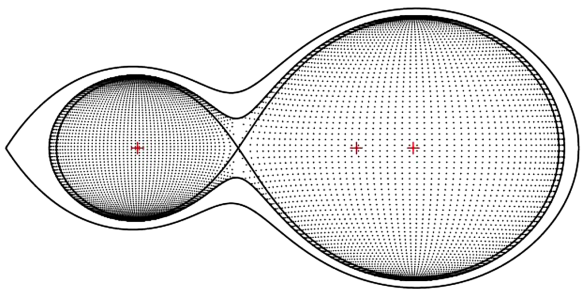

Figure 13. The Roche lobe surface of our solution.

9. Future work

Radial velocity curves are needed to obtain absolute (not relative) system parameters.

10. Acknowledgements

I would like to thank the American Association of Variable Star Observers for their support and for the services they supply to both amateurs and professionals alike.

References

Bradstreet, D. H., and Steelman, D. P. 2002, *Bull. Amer. Astron. Soc.*, **34**, 1224.

Centre de Donnees astronomiques de Strasbourg. 2007, SIMBAD Astronomical Database (http://simbad.u-strasbg.fr/simbad/).

Chamberlain, H., Samec, R., Caton, D., and Faulkner, D. 2020, *Bull. Amer. Astron. Soc.*, **52**, 114.02.

Christiansen, J. L., *et al.* 2008, *Mon. Not. Roy. Astron. Soc.*, **385**, 1749.

Guinan E. F., and Bradstreet D. H. 1988, in *Formation and Evolution of Low Mass Stars*, eds. A. K. Dupree, M. T. V. T. Lago, NATO Adv. Study Inst. Ser. C 241, Kluwer, Dordrecht, 345.

International Astronomical Union. 2013, International Earth Rotation and Reference Systems Service, International Celestial Reference System (ICRS; https://www.iers.org/IERS/EN/Science/ICRS/ICRS.html).

Kochanek, C. S., *et al.* 2017, *Publ. Astron. Soc. Pacific*, **129**, 104502.

Mikulášek, Z., Chrastina, M., Liška, J., Zejda, M., Janík, J., Zhu, L.-Y., and Qian, S.-B. 2014, *Contrib. Astron. Obs. Skalnaté Pleso*, **43**, 382.

Neustroev, V. 2017, "Astrophysics of Interacting Binary Stars" (http://vitaly.neustroev.net/teaching/2017b/astrophysics_of_interacting_binary_stars_02.pdf).

Samec, R. G., Labadorf, C. M., Hawkins, N. C., Faulkner, D. R., and Van Hamme, W. 2011, *Astron. J.*, **142**, 117.

Shappee, B. J., *et al.* 2014, *Astrophys. J.*, **788**, 48.

Terrell, D., and Wilson R. E. 2005, *Astrophys. Space Sci.*, **296**, 221.

Tylenda, R., and Kamiński, T. 2016, *Astron. Astrophys.*, **592A**, 134.

Van Hamme, W. V., and Wilson, R. E. 1998, *Bull. Amer. Astron. Soc.*, **30**, 1402.

Van Hamme, W., and Wilson, R. E. 2007, *Astrophys. J.*, **661**, 1129.

Watson, C., Henden, A. A., and Price, C. A. 2014, AAVSO International Variable Star Index VSX (Watson+, 2006–2014; http://www.aavso.org/vsx).

Wilson, R. E. 1979, *Astrophys. J.*, **234**, 1054.

Wilson, R. E. 1990, *Astrophys. J.*, **356**, 613.

Wilson, R. E. 1994, *Publ. Astron. Soc. Pacific*, **106**, 921.

Wilson, R. E. 2008, *Astrophys. J.*, **672**, 575.

Wilson, R. E. 2012, *Astron. J.*, **144**, 73.

Wilson, R. E., and Devinney, E. J. 1971, *Astrophys. J.*, **166**, 605.

Wilson, R. E., and Van Hamme, W. 2014, *Astrophys. J.*, **780**, 151.

Wilson, R. E., Van Hamme, W., and Terrell D. 2010, *Astrophys. J.*, **723**, 1469.